CANCER BIOTHERAPY AND RADIOPHARMACEUTICALS
Volume 35, Number 3, 2020

DOI: 10.1089/cbr.2019.2949

Enhancing Tumor Targeting Efficiency of Radiolabeled Uridine (via) Incorporation into Nanocubosomal Dispersions

Manal M. Sayed,[1] Hanan A. El-Sabagh,[1] Abdulaziz M. Al-mahallawi,[2,3] El-sayed Abd El-Halim,[1] Abeer M. Amin,[1] and Ahmed AbdEl-Bary[2]

Abstract

Background: Several nanosystems are currently being utilized to enhance the targeting efficiency of several cancer chemotherapeutic agents. This study was designed to improve tumor accumulation of iodine-125 (^{125}I)-uridine *via* incorporation into a nanocubosomal preparation.

Materials and Methods: Nanocubosomes were prepared with the aid of Glycerol mono-oleate and Pluronic F127. Each prepared nanocubosomal preparation was adequately characterized by testing their particle size, polydispersity index (PDI), ζ potential (ZP), and transmission electron microscopy. The radiolabeling of uridine with ^{125}I was attempted using several oxidizing agents to achieve a high radiochemical yield, and the factors affecting the reaction yield were studied in detail. A comparative biodistribution study of free ^{125}I-uridine and ^{125}I-uridine loaded nanocubosomes was performed in normal and tumor bearing mice. The biodistribution was evaluated by intravenous injection of the sterile test solution, and animals were anesthetized and dissected at different time intervals postinjection (p.i.).

Results: ^{125}I-uridine was obtained in a high radiochemical yield (92.5% ± 0.8%). Afterward, ^{125}I uridine was incorporated in a selected nanocubosome formulation, which showed nanosized cubic particles (178.6 ± 0.90 nm) with PDI (0.301 ± 0.04) and a ZP (34.35 ± 0.4). The biodistribution studies revealed that ^{125}I-uridine nanocubosomes showed higher tumor localization (3.1 ± 0.4%IA/g at 2 h p.i. and a tumor/muscle ratio of 6.2) compared with the free ^{125}I-uridine (2.7% ± 0.4%IA/g at 2 h p.i. and a tumor/muscle ratio of 3.3).

Conclusion: The results of this study confirmed that ^{125}I-uridine loaded nanocubosome had better efficiency in targeting the tumor site, which makes it an adequate targeting agent for tumor imaging.

Keywords: biodistribution, nanocubosomes, radioiodination, tumor targeting, uridine

Introduction

The development of less toxic and targeted therapeutic agents is of the outmost importance. Advanced nanotechnology has become an efficient tumor targeting modality. The use of such targeted agents will reduce the systemic side-effects by redirecting more of the drug dose toward the malignant sites, thus making anticancer treatment safer than conventional approaches.[1]

Self-assembled nanostructured preparations such as bicontinuous cubic liquid crystalline phases are currently in the focus for controlling the release of the incorporated pharmaceutical agents.[2] Nanocubosomes are nanostructures composed principally of amphiphilic polar lipid. When this amphiphilic substance dissolves in water with a concentration above the critical micelle concentration, it forms micellar aggregations where the micelles are forced to assume the cubic structure at higher concentrations.[3] In addition, heating is crucial to form that cubic crystalline liquid. As the polar heads remain intact and strongly bound together with hydrogen bonds, the hydrocarbon chain attached to them tends to melt at low temperatures.[4] In liquid crystalline state

[1]Department of Labeled Compounds, Hot Labs Center, Egyptian Atomic Energy Authority, Cairo, Egypt.
[2]Department of Pharmaceutics and Industrial Pharmacy, Faculty of Pharmacy, Cairo University, Cairo, Egypt.
[3]Department of Pharmaceutics, Faculty of Pharmacy, October University for Modern Science and Arts (MSA), Giza, Egypt.

Address correspondence to: Manal M. Sayed; Department of Labeled Compounds, Hot Labs Center, Egyptian Atomic Energy Authority; 3 Ahmed El Zomor Street, Cairo 202, Egypt
E-mail: **manal_moly@yahoo.com**

the carbon–carbon bonds tend to transform from all *trans* to *gauche* conformation.[5]

In the present study, glycerol mono-oleate (GMO) is a polar lipid, which is used in the formulation of nanocubosomes. GMO has a polar glycerol head and a lipophilic tail demonstrated in the C18 chain containing single double bond at C9.[6] Furthermore, GMO is a nontoxic, biodegradable, and biocompatible material, classified as generally recognized as safe (GRAS).[7] It is insoluble in an aqueous phase with hydrophilic–lipophilic balance = 3–4. Its solubility in water is $\approx 10^{-6}$ M and it forms a micellar solution with water above its critical aggregation concentration (4×10^{-6} M).[8]

Uridine is a ribonucleoside composed of a molecule of uracil attached to a ribofuranose moiety *via* a β-N^1-glycosidic bond. It contributes in the synthesis of RNA, glycogen, and biomembrane as it is a pyrimidine nucleoside. Uridine is crucial for proper brain function throughout the human life span and a variety of organs such as the reproductive organs, liver, and nervous systems.[9,10] Due to the high rate of protein synthesis, elevated levels of uridine base are found at tumor sites.[11] In addition, high level of uridine phosphorylase enzyme (UPase) was detected in different human solid tumors in comparison with surrounding normal tissues.[12,13] Thus, UPase can be considered as a potential marker for cancer diagnosis.[14] At the clinical level, uridine contributes in changing the cytotoxic effects of 5-fluorouracil in both normal and neoplastic tissues.[15]

Iodine-125 (^{125}I) emits both γ energy and Auger electron. Because of its low energy (35.5 KeV), it has large applications in cancer research. It has 60 days half life that permits the storage of the labeled compound for stability.[16]

The present study is the first to investigate the relevance of nanocubosomal formulation of uridine, containing GMO, as a novel potential nanosystem for tumor targeting. The aim of using the nanocubosomes is to improve uridine delivery into the targeted tumor sites upon intravenous (i.v.) application. Different variables affecting the nanocubosome characteristics were examined through the application of a full factorial design (2^3). The effects of different variables have been studied through determining the drug content percentage, particle size (PS) analysis, and ζ potential (ZP) measurements of the prepared systems. Transmission electron microscopy (TEM) was used to demonstrate the inherent morphological properties of the optimal formulation. The tumor targeting efficiency of uridine from the optimal uridine formulation was tested through radiolabeling of uridine with ^{125}I and biodistribution studies in normal and tumor bearing mice.

Materials and Methods

Materials

Uridine was purchased from Delta Pharma (Cairo, Egypt). GMO, Pluronic F108 (PF108), Pluronic F127 (PF127), methanol (high performance liquid chromatography [HPLC] grade), Chloramine-T (CAT), Iodogen, and *N*-Chlorosuccinimide (NCS) were obtained from Sigma-Aldrich (Germany). Potassium dihydrogen phosphate and disodium hydrogen phosphate were purchased from El-Nasr Pharmaceutical Chemicals Co. (Cairo, Egypt). All other chemicals and solvents were of analytical grade and used without a further purification. ^{125}I was purchased from the Institute of Isotopes Co., Ltd. (Budapest, Hungary), as no carrier solution.

Animals

Female Swiss albino mice weighing 20–25 g were obtained from the National Institute of Cancer (Cairo, Egypt). The animals were kept at constant environmental and nutritional conditions throughout the experimental period and kept at room temperature (25 ± 2) °C with a 12 h on/off light schedule. Female mice were used in this study due to their susceptibility to ehrlich ascites carcinoma (EAC) compared to males.[17] Animals were allowed free access to food and water all over the experiment.

Preparation of uridine loaded nanocubosomal dispersions

Preparing nanocubosomal dispersions was based on the emulsification of monoglyceride/surfactant mixtures in water.[18] On a hot plate adjusted at 70°C, GMO and the surfactant (PF108 or PF127) were melted. Afterward, the molten mixture was added dropwise to the aqueous solution of uridine maintained at 70°C under mechanical stirring at 1500 rpm.[18] Dispersions were maintained under stirring and were cooled to room temperature up to the solidification of lipid droplets. A full 2^3 factorial design was utilized to plan and analyze the experimental trials to select the optimal nanocubosomal formulation using Design-Expert® software (Stat-Ease, Inc., Minneapolis, MN). In this design, the surfactant type (X_1), surfactant percentage with respect to the dispersed phase (X_2), and the sonication time (X_3) were selected as independent variables, whereas PS (Y_1), polydispersity index (PDI) (Y_2), and ZP (Y_3) were chosen as dependent variables. The composition of the prepared uridine loaded nanocubosomes is presented in Table 2.

Determination of uridine content in nanocubosomes

One milliliter of uridine loaded nanocubosomal formulation was dissolved in methanol and sonicated for 10 min to have a clear solution. The concentration of uridine was measured spectrophotometrically at λ_{max} 260 nm. The following equation illustrates the calculation of the drug content percentage[19]:

$$Drug\ content = \frac{Actual\ yield}{Theoritical\ yield} \times 100 \qquad (1)$$

The calculated amount of uridine was considered as a reference of the total amount of drug for further studies.[20]

Determination of nanocubosomes PS, PDI, and ZP

Zetasizer Nano ZS (Malvern Instruments, Malvern, UK) according to the dynamic light scattering technology has been used for identifying the mean hydrodynamic diameter (z-average) and the PDI of uridine-loaded nanocubosomal dispersions. This was conducted using a helium-neon laser with a wavelength of 633 nm at 25°C ± 2°C. Based on the electrophoretic light scattering technology, the ZP values of the dispersions were estimated using a Laser Doppler Anemometer coupled with the same equipment. The samples were diluted with deionized water to adapt the signal level, and then measurements were carried out at room temperature

(25°C ± 0.5°C). The average of triplicate measurements of three independent samples was calculated.

TEM imaging of nanocubosomal dispersion

Morphology of the optimal nanocubosomal formula was visualized using TEM (JEM-1400; Jeol, Tokyo, Japan). One drop of diluted sample was placed on a carbon coated copper grid. It was stained by 2% w/v phosphotungstic acid (negative staining technique). The samples were investigated using TEM at 100 kV following to being dried at room temperature.

Radioiodination of uridine

Radioiodination of uridine, as well as the optimization of different factors affecting the radiochemical yield, was carried out. At the beginning, uridine solution in distilled water was prepared at a concentration of 1 mg/mL. The reaction was performed in tightly closed amber colored vials to which different amounts of uridine solution (equivalent to 50–300 μg uridine) were added. Then, different amounts of 1 mg/mL oxidizing agent aqueous solution (equivalent to 25–250 μg oxidizing agent) were added. Subsequently, 10 μL of ^{125}I (3.7 MBq) was added to the reaction mixture followed by shaking using an electric vortex. The reaction mixtures' pH values were adjusted at different values (2, 4, 7, 9, and 11) using different buffer solutions. The mixtures were, then, incubated at different temperatures (25°C, 40°C, 60°C, 80°C, and 100°C) for different time intervals (5, 15, 30, 45, and 60 min.). After the intended reaction time, 50 μL of $Na_2S_2O_3$ solution (20 mg/mL) was added to quench the reactive iodine.[21] Each factor was repeated thrice, and the differences in the values were statistically analyzed using one-way analysis of variance (ANOVA) with subsequent Tukey honestly significant difference test using SPSS software 19.0 (SPSS, Inc., Chicago, IL). The level of significance was set at $p \leq 0.05$.

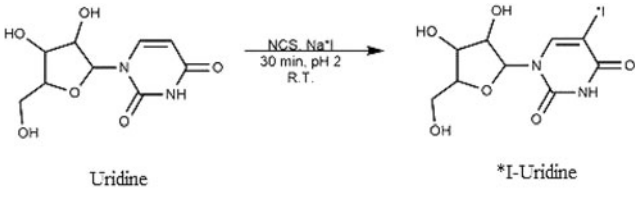

Radioiodination process of uridine`

Radiochemical analysis of the ^{125}I-uridine

Paper chromatography was used as a chromatographic method for qualitative determination of the radiochemical yield. Using Whatman paper number 1, 5 μL of the reaction mixture was placed 2 cm away from the paper base. A mixture of chloroform: methanol (3:1 v/v) was used for the development. After complete development, the paper was cut and dried and counted using a well type Na/Tl scintillation counter.

Table 1. Full Factorial Design (2^3) Used for the Optimization of the Uridine Nanocubosomal Formulations

Factors (independent variables)	*Levels*	
X_1: Type of surfactant	Pluronic F127	Pluronic F108
X_2: Surfactant percentage with respect to dispersed phase (%)	10	20
X_3: Sonication time (minutes)	10	20
Responses (dependent variables)	*Desirability constraints*	
Y_1: PS (nm)	Minimize	
Y_2: PDI	Minimize	
Y_3: ZP (mV)	Maximize (as absolute value)	

PDI, polydispersity index; PS, particle size; ZP, ζ potential.

Radiochemical yield was further confirmed by paper electrophoresis. The separation was done in accordance to the method reported earlier by Bayoumi et al.[22]

In addition, HPLC was done for purification using mobile phase of 0.05 mol/L phosphate buffer (potassium dihydrogen phosphate, adjusted pH to 3.5 by phosphate: methanol (98:2, v/v)) at a flow rate of 0.8 mL/min.[23]

Determination of in vitro stability of ^{125}I-uridine

The reaction mixtures were prepared at conditions that provided the maximum radiochemical yield. The experiment was carried out by allowing the HPLC purified compound to stand at ambient temperature and determine the yield percentage at different interval times (1, 2, 4, and 8 h).

Induction of tumor in mice and biodistribution study

The use of EAC as a model in anticancer research was proven by many authors to achieve accurate and reliable results.[24] EAC was maintained in female Swiss albino mice through weekly intraperitoneal transplantation. By needle aspiration EAC cells were obtained under aseptic condition. The ascitic fluid was diluted with sterile saline. Then, 0.2 mL of the diluted solution was injected intraperitoneally to produce ascites or intramuscularly in the left thigh of the mice to generate a solid tumor while the right thigh was kept as a control. Mice were kept for 7 to 10 days in a metabolic cage until the tumor progress was observed and used for further studies.[25] All experiments were conducted in accordance with the guidelines provided in the Egyptian Atomic Energy Authority and were approved by the animal ethics committee, Labeled Compounds Department, and the protocol of the studies was approved by the Research Ethics Committee in the Faculty of Pharmacy, Cairo University (Egypt).

Biodistribution of the ^{125}I-uridine and the ^{125}I-uridine loaded in the optimal nanocubosomal formula that was previously prepared as mentioned in Preparation of uridine loaded nanocubosomal dispersions with replacing of uridine with ^{125}I-uridine was performed in both healthy and tumor bearing Albino mice weighing about 25–30 g. Aliquots of 100 μL containing 3.7 MBq of saline solution of the HPLC purified ^{125}I-uridine and ^{125}I-uridine in the optimal nanocubosomal formula

Table 2. Experimental Runs, Independent Variables, and Measured Responses of the 2^3 Full Factorial Experimental Design of Uridine Nanocubosomal Formulations

Dispersions (D)	*X_1: Type of surfactant*	*X_2: Surfactant %*	*X_3: Sonication time (minutes)*	*Drug content*[a]	*Y_1: PS*[a] *(nm)*	*Y_2: PDI*[a]	*Y_3: ZP*[a] *(mV)*
D 1	Pluronic F127	10	10	95.22 ± 0.57	181.90 ± 4.10	0.291 ± 0.01	−30.55 ± 0.7
D 2	Pluronic F127	10	20	94.63 ± 0.98	245.85 ± 0.63	0.434 ± 0.03	−24.5 ± 0.04
D 3	Pluronic F127	20	10	97.84 ± 0.95	178.6 ± 0.32	0.301 ± 0.04	−34.35 ± 0.4
D 4	Pluronic F127	20	20	92.4 ± 0.42	421.45 ± 1.18	0.521 ± 0.02	−28.2 ± 0.77
D 5	Pluronic F108	10	10	93.6 ± 0.88	243.45 ± 0.7	0.292 ± 0.12	−26.95 ± 0.3
D 6	Pluronic F108	10	20	92.4 ± 0.65	193.9 ± 0.59	0.215 ± 0.01	−23.75 ± 0.2
D 7	Pluronic F108	20	10	96.11 ± 1.01	193.8 ± 0.91	0.3 ± 0.01	−28.8 ± 0.27
D 8	Pluronic F108	20	20	92.23 ± 0.29	194.85 ± 0.28	0.262 ± 0.01	−25.85 ± 0.5

[a]Data represented as mean ± standard deviation ($n = 3$).
PDI, polydispersity index; PS, particle size; ZP, ζ potential.

were injected i.v. into the tail vein of each mouse. The solution was sterilized by filtration through a Millipore filter (0.22 μm) into a sterile sealed vial before injection. Mice were anesthetized by chloroform at 0.5, 1, 2, 4, and 8 h postinjection (p.i.) after weighing. Blood, bone, and muscles were assumed to be 7%, 10%, and 40% of the total body weight, respectively.[26] Injected activity percentage per gram organ or body fluid (%IA/g ± standard deviation) in a population of 3 mice for each time point was reported. Data were evaluated with one-way ANOVA test. The level of significance was set at $p < 0.05$.

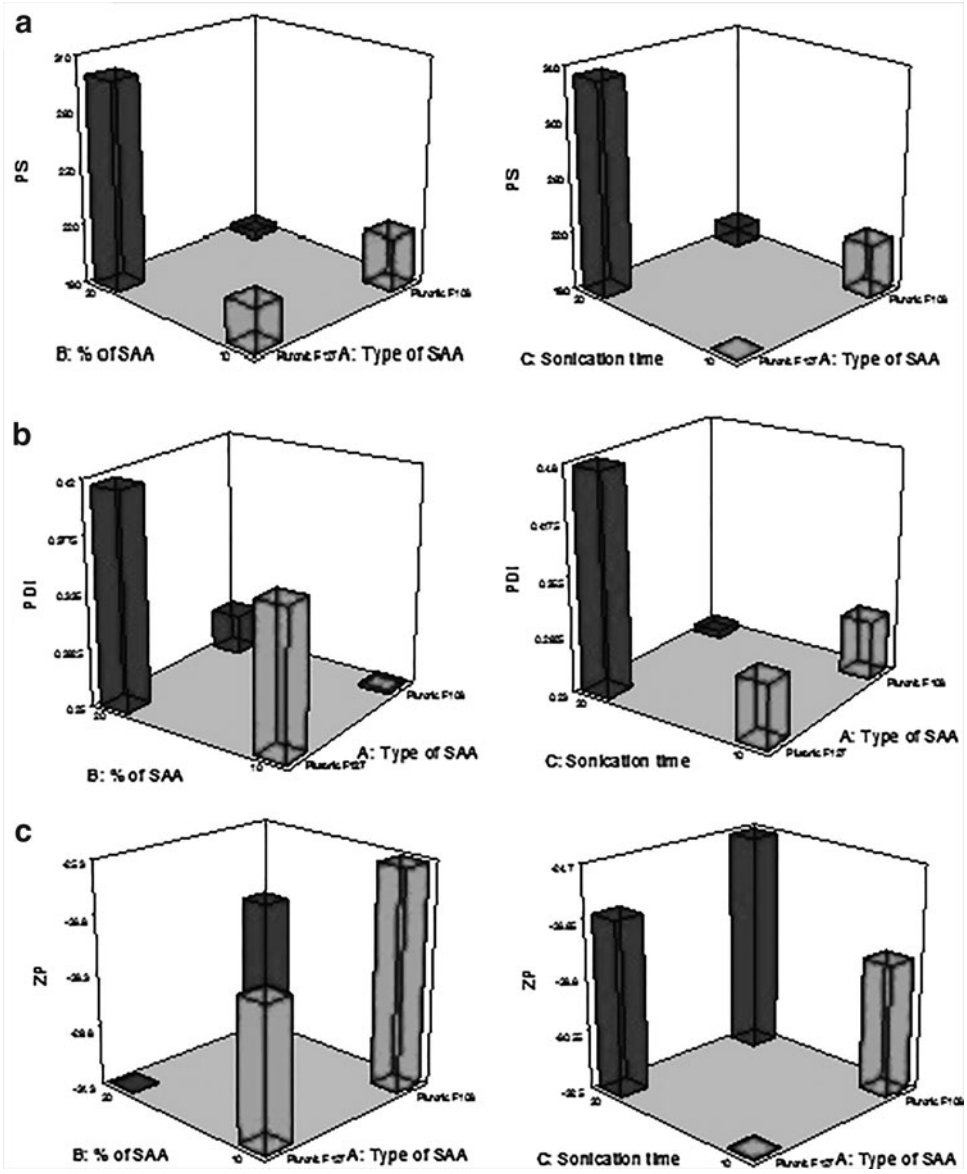

FIG. 1. Response three-dimensional plots for the effect of type of SAA (A), % of SAA (B), and Sonication time (C) on **(a)** PS, **(b)** PDI, and **(c)** ZP of the cubosomal dispersion formulae. PDI, polydispersity index; PS, particle size; SAA, surface active agent; ZP, ζ potential.

Results

Preparation of uridine loaded nanocubosomal dispersions

For the preparation of nanocubosomal formulation, a full 2^3 factorial design with statistical analysis through Design-Expert software was used. Satisfied precision measured the signal to noise ratio to ensure that the model can be used to navigate the design space.[27] A ratio >4 (the desirable value) was observed in all responses. Moreover, the predicted R^2 was calculated as a measure of how good the model predicts a response value.[28,29] The adjusted and predicted R^2 values should be within ~ 0.20 of each other to be in a quite good agreement, and this was accomplished in the investigated responses.[30,31] Nanocubosomal dispersions had drug content ranging from 92.23% to 97.84% that were insignificantly different from the added amount of uridine as shown in Table 1.

Determination of nanocubosomes PS, PDI, and ZP

The PS values of the prepared dispersions are presented in Table 2 as *z*-average diameter, which represents the mean hydrodynamic diameter of the particles.[32] It was observed that the dispersions were in the nanoscale range as their PS ranged between 178.6 ± 0.32 and 421.45 ± 1.18 nm with a PDI of <1. From a statistical analysis it was showed that the type of surfactant (X_1) significantly influences the PS and PDI of the dispersions ($p = 0.0146$ and 0.0101). Moreover, sonication time (X_3) had a significant effect on PS ($p < 0.05$). The PS of the dispersions increased proportionally with increasing the sonication time as presented in Figure 1a and b. In the present investigation, the obtained ZP values form the prepared dispersions ranging from -23.75 ± 0.2 to -34.35 ± 0.4 mV (Table 2).

TEM imaging of nanocubosomal dispersion

The morphology was examined using TEM to confirm the formation of cubic structures in the prepared dispersions (Figure 2). Micrographs revealed that the particles were cubic in shape and well separated from each other. The TEM showed that the prepared cubosomes are in the nanosize, which confirms the results of particle size measurement.

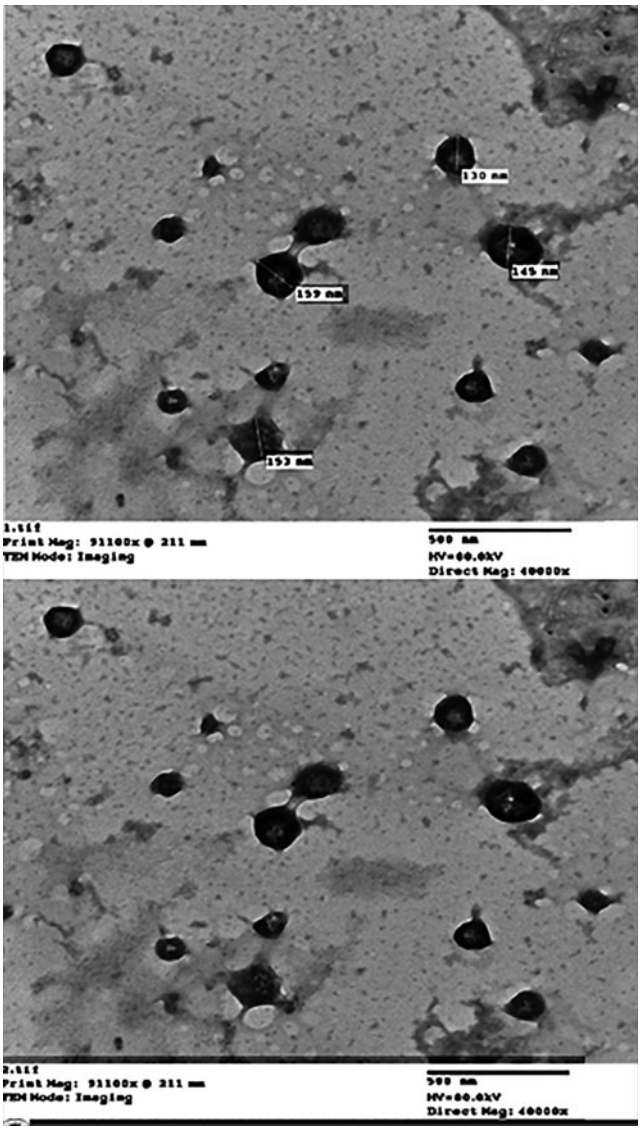

FIG. 2. Transmission electron micrographs of optimal nanocubosomal dispersion; the cubosomes are cubic in shape, nanosized, and well separated from each other.

Radioiodination of uridine

Concerning the radiolabeling of uridine, the radiochemical purity of the ^{125}I-uridine was determined using paper chromatography where the radioiodide (I^-) remained near the origin ($R_f = 0$–0.1), while the ^{125}I-uridine moved with the solvent front ($R_f = 0.8$–1). Radiochemical purity was further confirmed by paper electrophoresis where ^{125}I-uridine remained at the spotting point indicating its neutral charge, while the free radioiodide (I^-) moves toward the anode by a distance from spotting point that equals to 14 cm.

The radioiodination method was optimized by studying the effect of using different amounts of variable oxidizing agents and uridine itself, the pH of the reaction, reaction temperature, and reaction time. The collective results are shown in Figure 3. As can be deduced from the figure, the use of CAT and iodogen as oxidizing agents gave low radiochemical yield. In contrast, NCS showed better radiochemical yield ($92.5\% \pm 0.8\%$ at 10 μg) compared to CAT and iodogen.

Varying the amount of uridine added to the reaction had a significant effect on the radiochemical yield, whereas the optimum amount was found to be 250 μg of uridine. Any further increase in uridine amount did not increase the radiochemical yield. The use of alkaline pH medium had a negative effect on the radiochemical yield, which can be attributed to the formation of undesired radioiodine species (hypoiodite and iodate).[33] The maximum radiochemical yield was obtained at pH value of 2. Furthermore, the reaction showed highest yields at ambient temperature; slight heating or boiling caused a drastic decrease in the radiochemical yield which can be attributed to the thermal decomposition of the radiolabeled product. In addition, the reaction yield increased with time and reached its optimum at 30 min. The yield slightly decreased afterward which can

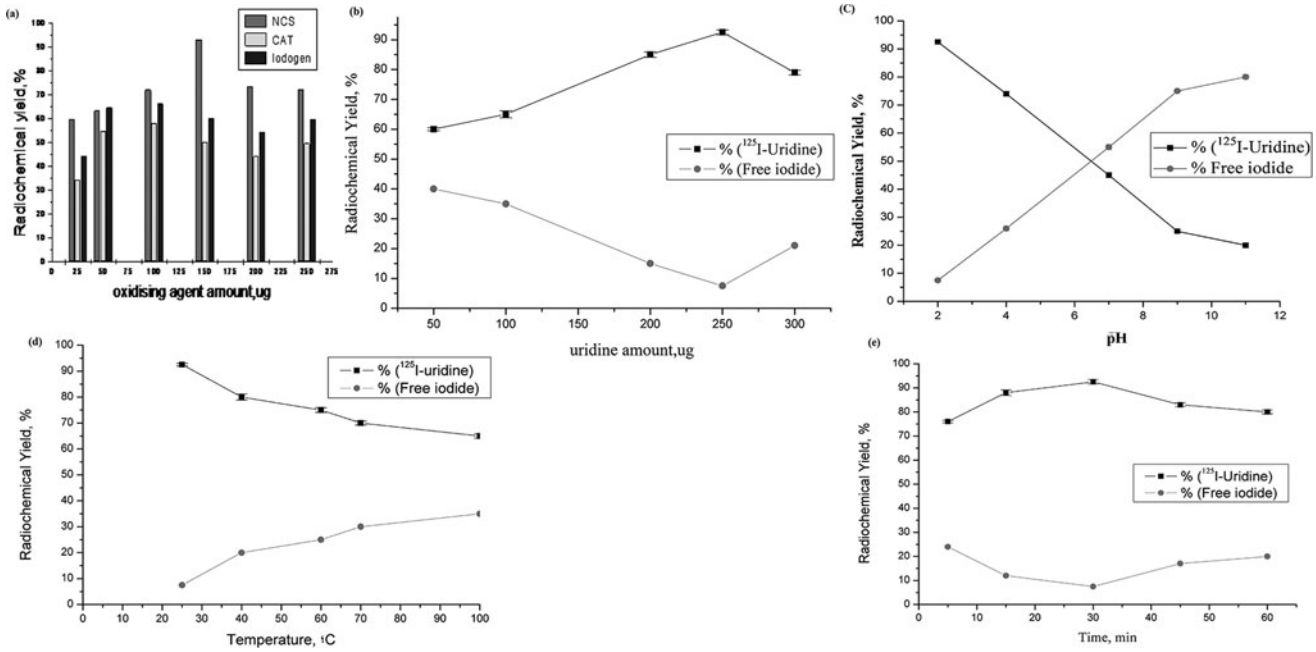

FIG. 3. Variation of the radiochemical yield of ^{125}I-uridine as a function of **(a)** type and concentration of oxidizing agents, **(b)** uridine amount (μg), **(c)** pH of the reaction mixture, **(d)** reaction mixture temperature (°C), and **(e)** reaction time (minutes). CAT, Chloramine-T; NCS, *N*-Chlorosuccinimide.

be explained by the degradation of uridine due to long exposure to NCS.

The results of the *in vitro* stability revealed that the ^{125}I-uridine had an acceptable stability up to 12 h post-labeling as presented in Figure 4.

Radiochemical analysis of the ^{125}I-uridine

The radiochromatogram of ^{125}I-uridine obtained by HPLC separation on RP-C18 column at the optimum conditions is shown in Figure 5. Based on the determination of the radioactivity, two peaks were detected at $R_t = 2.5$ and 5.5 min corresponding to free iodide and ^{125}I-uridine, respectively. Upon injection of the standard uridine, a peak at $R_t = 4$ min was obtained. The collected fractions containing the ^{125}I-uridine were evaporated to dryness, dissolved in physiological saline, and sterilized by filtration using 0.22 μm Millipore filter. The purified sterile solution was used for the biodistribution study.

Biodistribution study

The biodistribution of each of free ^{125}I-uridine and its nanocubosomal formulation was studied in normal and solid tumor bearing mice following i.v. administration. In normal mice, ^{125}I-uridine showed rapid blood clearance ($9.7 \pm 0.3\%$ IA/g and $4.6 \pm 0.4\%$IA/g at 0.5 and 2 h p.i., respectively), Figure 6. Elevated levels of activity were observed ($14.33 \pm 0.1\%$IA/g at 0.5 h p.i.) in the kidneys, which reached a maximum level of $22.8 \pm 0.3\%$IA/g at 2 h p.i. This was accompanied by high radioactivity of the collected urine samples.

The thyroids showed minimal uptake, which increased slightly with time. The biodistribution of ^{125}I-uridine solution in tumor bearing mice showed similar pattern as in normal mice (Fig. 7). The tumor uptake of ^{125}I-uridine increased gradually with maximum uptake at 2 h p.i. ($2.7 \pm 0.4\%$IA/g).

In contrast, biodistribution of ^{125}I-uridine nanocubosome in normal mice showed high levels in Reticular Endothelial System (RES), Figure 8. It was observed that it exhibited relatively higher residence time in blood compared with ^{125}I-uridine solution. Compared with the free drug, ^{125}I-uridine loaded nanocubosome was shown to have higher tumor targeting as shown from Figure 9.

Discussion

The factorial designs are used to recognize the variables that might affect the properties of a new drug delivery system. These designs analyze the effect of different variables on the characteristics of the drug delivery system.[34] In this article,

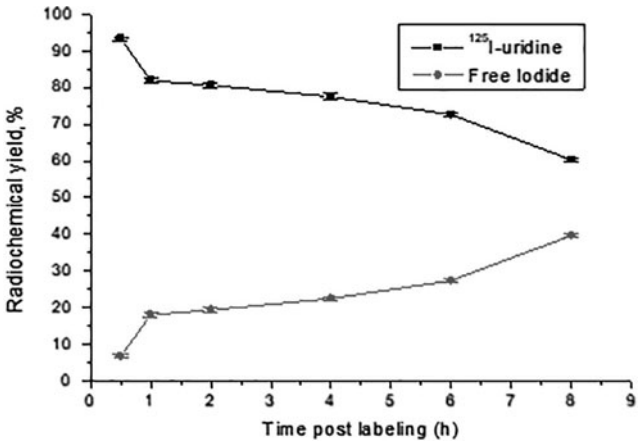

FIG. 4. *In vitro* stability of ^{125}I-uridine.

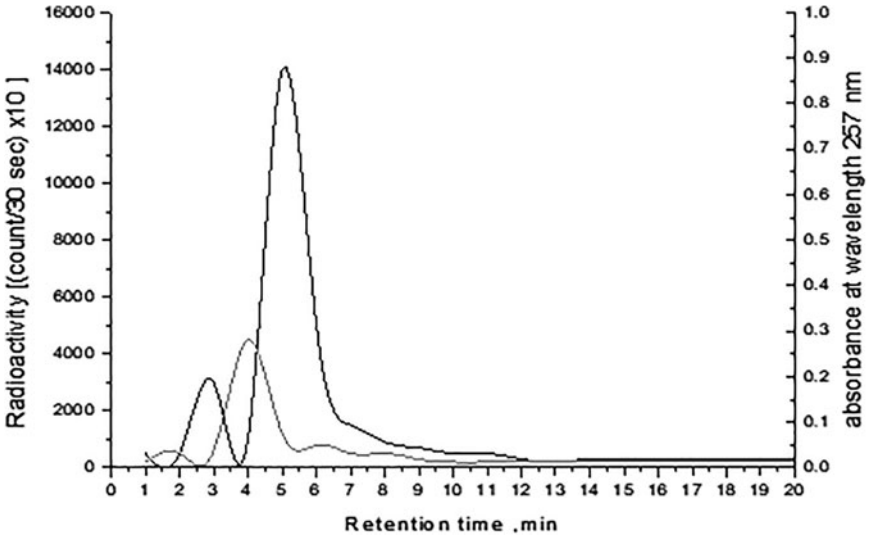

FIG. 5. High performance liquid chromatography chromatogram of iodinated uridine.

preliminary trials (data not shown) were performed to determine the probable ranges of the independent variables.

Nanoscale drug delivery systems have shown high accumulation in solid tumor and improved retention time.[35] The stabilizing effect of PF127 is attributed to the balance between the hydrophobic domain size of Poly Propylene Oxide (PPO) that is responsible for the anchoring to lipid bilayers and the hydrophilic chain length of Poly Ethylene Oxide (PEO) that is oriented toward the aqueous medium and acts as a steric barrier to prevent aggregation of nanoparticles. In contrast, the surfactant ratio (X_2) had insignificant effect on average PS and PDI of nanocubosomes ($p < 0.05$). As illustrated in Table 2, increasing the concentration of surfactant from 10 to 20 led to insignificant decrease in average PS. The surfactant molecules might be unable to cover the whole particle surface allowing for the aggregation of some particles till their surface area is decreased to a point that the limited surfactant concentration could coat the entire agglomerate surface and, consequently, form a stable dispersion with relatively larger particles.[36] The higher surfactant concentration, with respect to fixed GMO concentrations, would allow for the partitioning of more surfactant molecules into the interfacial domain of the liquid crystalline phase. This leads to more steric stabilization and lower tendency for aggregation.[37]

Generally, the system is considered stable when ZP (the measure of the overall charges acquired by vesicles) value is around ±30 mV due to electric repulsion between particles.[38] These values relatively indicate the strong electric repulsion between particles and the lowered tendency toward aggregation.

Variation in ZP will be discussed in terms of its absolute value to avoid misperception, as all the formulations in the current study had negative ZP.[39] The ANOVA results

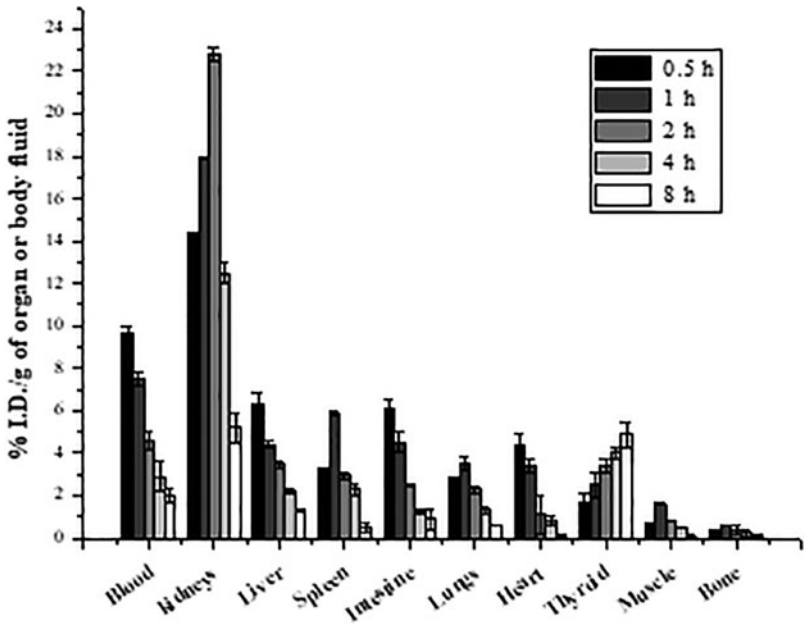

FIG. 6. Biodistribution of ^{125}I-uridine in normal albino mice at different time intervals postinjection (%ID/g of organ or body fluid ± standard deviation, ($n = 3$).

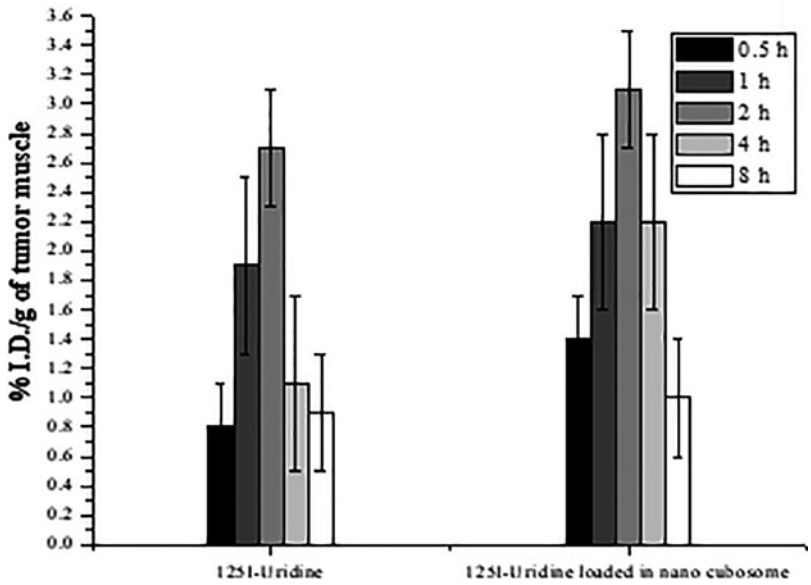

FIG. 7. Tumor uptake of ^{125}I-uridine and ^{125}I-uridine loaded in nanocubosome at different time intervals postinjection.

revealed the direct correlations between the ZP values and surfactant percentage with respect to dispersed phase (%). This could be due to the ionization of the negatively charged carboxylic groups of the fatty acid moieties within GMO or PF127 as presented in Figure 1c.

According to the full factorial design, Design-Expert software was used to select the optimized formulation from the prepared 8 formulations. The criteria set for the optimum formulation [achieving maximum value of ZP (absolute value) and minimum values for PS and PDI] were established in formulation D3, which was prepared using 20% PF127 in the dispersed phase and was sonicated for 10 min. This formulation revealed a PS of 178.6 ± 0.32 nm, PDI of 0.301 ± 0.04, and ZP of -34.35 ± 0.4 mV. The TEM shows that the prepared nanocubosomes are in the nanosize, which confirms the results of particle size measurement (Table 2).

The radioiodination of uridine was conducted using electrophilic substitution method. Results of radiochemical yield from the two separation methods (paper chromatography and paper electrophoresis) were almost similar and were confirmed by HPLC.

The *in vitro* stability study was conducted to determine the degree of radiolysis on ^{125}I-uridine and the suitable injection and indicated that ^{125}I-uridine was relatively stable at ambient temperature.

The biodistribution patterns of free ^{125}I-uridine showed rapid blood clearance and primary excretion through the kidneys.[40] Low levels of thyroid uptake showed minimal

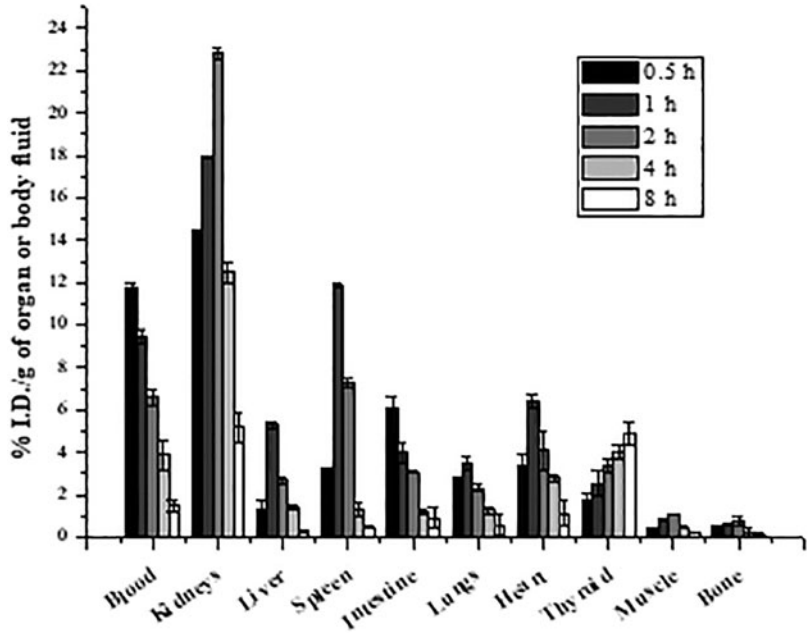

FIG. 8. Biodistribution of ^{125}I-uridine loaded cubosome in normal albino mice at different time intervals postinjection (%ID/g of organ or body fluid ± standard deviation, $n = 3$).

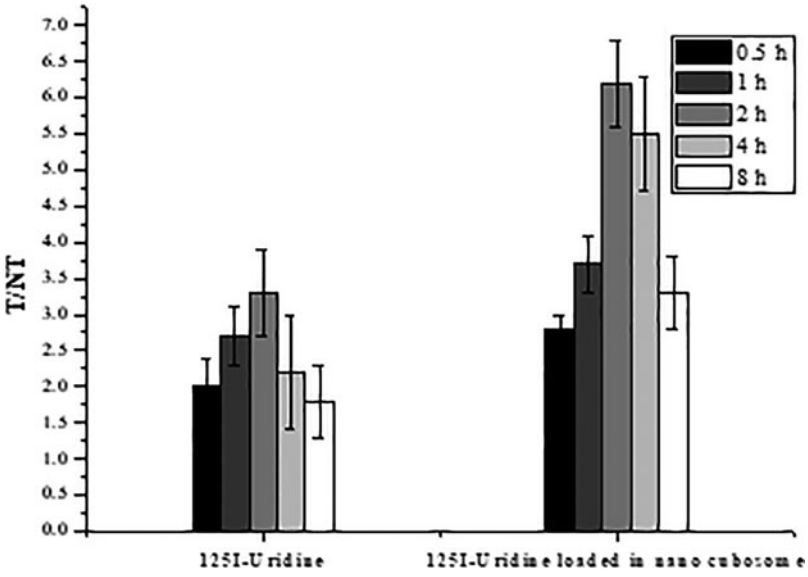

FIG. 9. T/NT of ^{125}I-uridine and ^{125}I-uridine loaded in nanocubosome. T/NT, tumor/normal tissue ratio.

in vivo deiodination of ^{125}I-uridine.[41] It was revealed that ^{125}I-uridine nanocubosomes showed higher tumor localization (3.1 ± 0.4%IA/g at 2 h p.i. and a tumor/muscle ratio of 6.2) compared with the free ^{125}I-uridine (2.7 ± 0.4%IA/g at 2 h p.i. and a tumor/muscle ratio of 3.3).

Using nanocubosomal formulation resulted in higher tumor targeting and overall slower blood clearance and excretion. The results of the comparative biodistribution study provided a compelling evidence that the use of nanocubosomes has enhanced the accumulation of uridine at tumor sites.

Conclusion

Uridine was successfully labeled with ^{125}I by direct electrophilic substitution reaction giving radiochemical yield of $92.5\% \pm 0.8\%$. ^{125}I-uridine showed a reasonable *in vitro* stability. The optimal nanocubosomal dispersion formula revealed small PS, PDI, and high ZP. Biodistribution analysis in tumor bearing mice revealed that the maximum tumor/muscle ratio of ^{125}I-uridine loaded in nanocubosomal dispersions was comparable to the promising ratio of the ^{125}I-uridine. Based on these studies, radioiodination of uridine with iodine and loading in nanocubosomes could be of promising value as a novel tumor targeting agent.

Disclosure Statement

There are no existing financial conflicts.

Funding Information

No funding was received for this article.

References

1. Holtz RD, Lima BA, Souza Filho AG, et al. Nanostructured silver vanadate as a promising antibacterial additive to water-based paints. Int J Nanomedicine 2012;8:935.
2. Drummond CJ, Fong C. Surfactant self-assembly objects as novel drug delivery vehicles. Curr Opin Colloid Interface Sci 1999;4:449.
3. Milak S, Zimmer A. Glycerol monooleate liquid crystalline phases used in drug delivery systems. Int J Pharm 2015; 478:569.
4. Larsson K. Aqueous dispersions of cubic lipid–water phases. Curr Opin Colloid Interface Sci 2000;5:64.
5. Garti N, Libster D, Aserin A. Lipid polymorphism in lyotropic liquid crystals for triggered release of bioactives. Food Funct 2012;3:700.
6. Ganem-Quintanar A, Quintanar-Guerrero D, Buri P. Monoolein: A review of the pharmaceutical applications. Drug Dev Ind Pharm 2000;26:809.
7. Bode JC, Kuntsche J, Funari SS, et al. Interaction of dispersed cubic 1519 phases with blood components. Int J Pharm 2013;448:87.
8. Barauskas J, Cervin C, Jankunec M, et al. Interactions of lipid-based liquid crystalline nanoparticles 1508 with model and cell membranes. Int J Pharm 2010;391:284.
9. Cansev M. Uridine and cytidine in the brain: Their transport and utilization. Brain Res Brain Res Rev 2006;52:389.
10. Wurtman RJ, Ulus IH, Cansev M, et al. Synaptic proteins and phospholipids are increased in gerbil brain by administering uridine plus docosahexaenoic acid orally. Brain Res 2006;1088:83.
11. Tezuka M, Tamemasa O. Incorporation characteristics of uracil, uridine, and orotic acid into ribonucleic acid of neoplastic cells. Gan 1977;68:287.
12. Kanzaki A, Takebayashi Y, Bando H, et al. Expression of uridine and thymidine phosphorylase genes in human breast carcinoma. Int J Cancer 2002;97:631.
13. Cao D, Ziemba A, McCabe J, et al. Differential expression of uridine phosphorylase in tumors contributes to an improved fluoropyrimidine therapeutic activity. Mol Cancer Ther 2011;10:2330.
14. Watanabe S, Uchida T. Cloning and expression of human uridine phosphorylase. Biochem Biophys Res Commun 1995;216:265.
15. Yamamoto T, Koyama H, Kurajoh M, et al. Biochemistry of uridine in plasma. Clin Chim Acta 2011;18:41219.

16. Makrigiorgos G, Adelstein S, Kassis A. Auger electrons emitters: Insights gained from in vitro experiments. J Radiat Environ Biophys 1990;29:5.
17. Vincent PC, Nicholls A. Comparison of the growth of the Ehrlich Ascites Tumor in male and female mice. Cancer Res 1967;27:1058.
18. Esposito E, Eblovi N, Rasi S, et al. Lipid-based supramolecular systems for topical application: A preformulatory study, AAPS Pharm Sci 2003;5:E30.
19. Morsi NM, Abdelbary GA, Ahmed MA. Silver sulfadiazine based nanocubosome hydrogels for topical treatment of burns: Development and in vitro/in vivo characterization. Eur J Pharm Biopharm 2014;86:178.
20. Esposito E, Cortesi R, Drechsler M, et al. Nanocubosome dispersions as delivery systems for percutaneous administration of indomethacin. Pharm Res 2005;22:2163.
21. Greenwood N, Earnshaw A. Chemistry of the Elements, 2nd Edition. United Kingdom: Elsevier Ltd., 1997.
22. Bayoumi NA, Amin AM, Ismail NSM, et al. Radioiodination and biological evaluation of cladribine as potential agent for tumor imaging and therapy. Radiochim Acta 2015;103:777.
23. Elmaleh DR, John WB. (2001)US patent 6,187,286 (2013).
24. Sheeja KR, Kuttan G, Kuttan R. Cytotoxic and antitumor activity of Berberin. Amala Res Bull 1997;17:73.
25. Arulsudar N, Subramanian N, Mishra P, et al. Preparation, characterization, and biodistribution study of technetium-99m labeled leuprolide acetate-loaded liposomes in ehrlich ascites tumor-bearing mice. AAPS Pharm Sci 2004;61:45.
26. Rhodesm BA. Considerations in the radiolabeling of albumin. J Nucl Med 1974;25:281.
27. de Lima LS, Araujo MDM, Quináia SP, et al. Adsorption modeling of Cr, Cd and Cu on activated carbon of different origins by using fractional factorial design. Chem Eng J 2011;166:881.
28. Chauhan B, Gupta R. Application of statistical experimental design for optimization of alkaline protease production from *Bacillus* sp. RGR-14. Process Biochem 2004;39:2115.
29. Kaushik R, Saran S, Isar J, et al. Statistical optimization of medium components and growth conditions by response surface methodology to enhance lipase production by *Aspergillus carneus*. J Mol Catal B Enzym 2006;40:121.
30. Annadurai G, Ling LY, Lee J-F. Statistical optimization of medium components and growth conditions by response surface methodology to enhance phenol degradation by *Pseudomonas putida*. J Hazard Mater 2008;151:171.
31. Bendas ER, Abdelbary AA. Instantaneous enteric nanoencapsulation of omeprazole: Pharmaceutical and pharmacological evaluation. Int J Pharm 2014;468:97.
32. Das S, Ng WK, Tan RB. Are nanostructured lipid carriers (NLCs) better than solid lipid nanoparticles (SLNs): Development, characterizations and comparative evaluations of clotrimazole-loaded SLNs and NLCs? Eur J Pharm Sci 2012;47:139.
33. El-Tawoosy M, Farouk N, El-Bayoumy AS. Labeling of atenolol with radioactive iodine-125 using N-bromosuccinimide and hydrogen peroxide as oxidizing agents. J Radioanal Nucl Chem 2011;290:595.
34. Araujo J, Gonzalez-Mira E, Egea MA, et al. Optimization and physicochemical characterization of a triamcinolone acetonide-loaded NLC for ocular antiangiogenic applications. Int J Pharm 2010;393:167.
35. Waitea CL, Roth CM. Nanoscale drug delivery systems for enhanced drug penetration into solid tumors: Current progress and opportunities. Crit Rev Biomed Eng 2012; 40:21.
36. Ghorab DM, Amin MM, Khowessah OM, et al. Colontargeted celecoxib-loaded Eudragit_ S100-coated poly-e-caprolactone microparticles: Preparation, characterization and in vivo evaluation in rats. Drug Deliv 2011;18:523.
37. Madheswaran T, Baskaran R, Yong CS, et al. Enhanced topical delivery of finasteride using glyceryl monooleate-based liquid crystalline nanoparticles stabilized by cremophor surfactants. AAPS PharmSciTech 2014;15:44.
38. Souto EB, et al. Fundamental of pharmaceutical nanoscience. Springer, United States, Part I, 2013.
39. Abdelbary AA, Li X, El-Nabarawi M, et al. Effect of fixed aqueous layer thickness of polymeric stabilizers on zeta potential and stability of aripiprazole nanosuspensions. Pharm Dev Technol 2013;18:730.
40. Kim E, Kang W. Pharmacokinetics of uridine following ocular, oral and intravenous administration in rabbits. Biomol Ther 2013;21:170.
41. El-Gogary SR, Waly MA, Ibrahim IT, et al. Synthesis and UV absorption of new conjugated quinoxaline 1,4-dioxide derivative anticipated as tumor imaging and cytotoxic agents. Monatsh Chem 2010;141:1253.